

Syracuse University

SURFACE at Syracuse University

Physics - All Scholarship

Physics

Winter 12-5-2021

Extracellular Vimentin as a Target Against SARS-CoV-2 Host Cell Invasion

Łukasz Suprewicz
Medical University of Białystok

Maxx Swoger
Syracuse University

Sarthak Gupta
Syracuse University

Ewelina Piktel
Medical University of Białystok

Fitzroy J. Byfield
University of Pennsylvania

See next page for additional authors

Follow this and additional works at: <https://surface.syr.edu/phy>



Part of the [Physics Commons](#)

Recommended Citation

Suprewicz, Ł., Swoger, M., Gupta, S., Piktel, E., Byfield, F. J., Iwamoto, D. V., Germann, D., Reszeć, J., Marcińczyk, N., Carroll, R. J., Janmey, P. A., Schwarz, J. M., Bucki, R., Patteson, A. E., Extracellular Vimentin as a Target Against SARS-CoV-2 Host Cell Invasion. *Small* 2022, 18, 2105640. <https://doi.org/10.1002/smll.202105640>

This Article is brought to you for free and open access by the Physics at SURFACE at Syracuse University. It has been accepted for inclusion in Physics - All Scholarship by an authorized administrator of SURFACE at Syracuse University. For more information, please contact surface@syr.edu.

Author(s)/Creator(s)

Łukasz Suprewicz, Maxx Swoger, Sarthak Gupta, Ewelina Piktel, Fitzroy J. Byfield, Daniel V. Iwamoto, Danielle Germann, Joanna Reszeć, Natalia Marcińczyk, Robert J. Carroll, Paul A. Janmey, J. M. Schwarz, Robert Bucki, and Alison E. Patteson

Extracellular Vimentin as a Target Against SARS-CoV-2 Host Cell Invasion

Łukasz Suprewicz, Maxx Swoger, Sarthak Gupta, Ewelina Piktel, Fitzroy J. Byfield, Daniel V. Iwamoto, Danielle Germann, Joanna Reszeć, Natalia Marcińczyk, Robert J. Carroll, Paul A. Janmey, J. M. Schwarz, Robert Bucki,* and Alison E. Patteson*

Infection of human cells by pathogens, including SARS-CoV-2, typically proceeds by cell surface binding to a crucial receptor. The primary receptor for SARS-CoV-2 is the angiotensin-converting enzyme 2 (ACE2), yet new studies reveal the importance of additional extracellular co-receptors that mediate binding and host cell invasion by SARS-CoV-2. Vimentin is an intermediate filament protein that is increasingly recognized as being present on the extracellular surface of a subset of cell types, where it can bind to and facilitate pathogens' cellular uptake. Biophysical and cell infection studies are done to determine whether vimentin might bind SARS-CoV-2 and facilitate its uptake. Dynamic light scattering shows that vimentin binds to pseudovirus coated with the SARS-CoV-2 spike protein, and antibodies against vimentin block in vitro SARS-CoV-2 pseudovirus infection of ACE2-expressing cells. The results are consistent with a model in which extracellular vimentin acts as a co-receptor for SARS-CoV-2 spike protein with a binding affinity less than that of the spike protein with ACE2. Extracellular vimentin may thus serve as a critical component of the SARS-CoV-2 spike protein-ACE2 complex in mediating SARS-CoV-2 cell entry, and vimentin-targeting agents may yield new therapeutic strategies for preventing and slowing SARS-CoV-2 infection.

enzyme 2 (ACE2), for cell entry.^[1,2] The ACE2 receptor is expressed in a plethora of tissues, including the lung, kidney, gastrointestinal tract, and vascular endothelium, which all serve as sites for SARS-CoV-2 infection.^[3] While ACE2 is required for SARS-CoV and SARS-CoV-2 infection, it does not appear solely sufficient. The expression of ACE2 in the human respiratory system is low compared to other organs^[4–6] and while the affinity of the SARS-CoV-2 spike protein with ACE is especially strong, the binding-on rate is slow.^[1] At the super-physiological concentrations above nM used in vitro, the half time of maximal binding for SARS-CoV-2 is around 30 s, and the concentration in vivo is substantially lower. These findings have given rise to an emerging hypothesis of a critical co-receptor that facilitates binding of the SARS-CoV-2 virus and its delivery to ACE2,^[7] and several possible SARS-CoV-2 co-receptor candidates have been found, including neuropilins,^[8] heparan sulfate,^[9] and sialic acids.^[10] The ongoing coronavirus disease 2019 (COVID-19) pandemic and the threat of future coronavirus outbreaks underscore the need to identify the precise entry mechanism used by the SARS-CoV-2 virus to develop protective strategies against it.

1. Introduction

Infection of human cells by pathogens, including the severe acute respiratory syndrome coronavirus 2 (SARS-CoV-2), proceeds by a series of cell surface protein binding and membrane fusion events that are usually centered on a crucial receptor. The SARS-CoV-2 virus is genetically similar to SARS-CoV (SARS) and uses the SARS-CoV receptor, angiotensin-converting

Here, we report that cell surface vimentin acts as a co-receptor for SARS-CoV-2 host cell invasion and that antibodies against vimentin can block up to 80% of the cellular uptake


Ł. Suprewicz, E. Piktel, R. Bucki
Department of Microbiological and Nanobiomedical Engineering
Medical University of Białystok
Mickiewiczza 2C, Białystok 15-089, Poland
E-mail: buckirobert@gmail.com

M. Swoger, S. Gupta, D. Germann, R. J. Carroll, J. M. Schwarz,
A. E. Patteson
Physics Department and BioInspired Institute
Syracuse University
140 Sims Dr, Syracuse, NY 13244, USA
E-mail: aepattes@syr.edu

F. J. Byfield, D. V. Iwamoto, P. A. Janmey, R. Bucki
Institute for Medicine and Engineering and Department of Physiology
1010 Vagelos Research Laboratories
University of Pennsylvania
3340 Smith Walk, Philadelphia, PA 19104, USA

J. Reszeć
Department of Medical Pathomorphology
Medical University of Białystok
Białystok PL-15269, Poland
N. Marcińczyk
Department of Biopharmacy
Medical University of Białystok
Mickiewiczza 2C, Białystok 15-089, Poland

J. M. Schwarz
Indian Creek Farm
1408 Trumansburg Road, Ithaca, NY 14850, USA

 The ORCID identification number(s) for the author(s) of this article can be found under <https://doi.org/10.1002/smll.202105640>.

DOI: 10.1002/smll.202105640

of SARS-CoV-2 pseudovirus. While cell surface vimentin is an unconventional target for viruses, there are now numerous studies implicating its role in the binding and uptake of multiple different viruses,^[11–18] including the SARS-CoV virus,^[19] suggesting it might also be involved in cell host invasion by SARS-CoV-2. Interestingly, the expression of SARS-CoV-2 entry factors, ACE2 and transmembrane serine protease 2 (TMPRSS2), is particularly high in nasal epithelial goblet secretory cells and ciliated cells,^[20,21] on which immunohistological studies have shown the presence of vimentin.^[22] We show here that extracellular vimentin is also present in healthy adult lung tissue and detail the numerous routes by which it might arise in the lung, the respiratory tract, and other tissues. We demonstrate that vimentin binds to SARS-CoV-2 pseudoviruses that are equipped with SARS-CoV-2 spike protein via dynamic light scattering (DLS) and atomic force microscopy (AFM) and propose a novel mechanism in which non-vimentin expressing cells can acquire vimentin released into the extracellular environment by neutrophil netosis. Motivated by our experimental results, we present a novel coarse-grain model that captures the main features of membrane wrapping, treating extracellular vimentin as a co-receptor that mediates cell-virus interactions. Our work highlights extracellular vimentin as a potential target against SARS-CoV-2 that could block the spread of COVID-19 and potentially other infectious diseases caused by viruses and bacteria that exploit cell surface vimentin for host invasion.

2. Results

2.1. Presence of Extracellular Vimentin in Human Lung, Airway Fluids, and Fat Tissue

Vimentin is an unexpected target for SARS-CoV-2 viral entry into host cells lining the nasal and lung epithelial airways (Figure 1). Intermediate filaments (IFs) are categorized into five types based on similarities in sequence, which also exhibit similarities in tissue origin.^[23,24] Keratin is the main IF protein expressed in epithelial cells, whereas vimentin is expressed in mesenchymal cells such as fibroblasts, endothelial cells, and leukocytes. While vimentin is not nascently expressed in epithelial cells, its expression can occur in transformed cells associated with cancer, fibrosis, or immortalized cell lines.

There are however many routes by which vimentin might occupy the extracellular space of the lung and other tissues. Lung epithelial cells are capable of expressing vimentin. This occurs, for instance, if the cell becomes fibrotic, cancerous, or undergoes the epithelial to mesenchymal transition. However, the source of extracellular vimentin need not be the lung epithelial cell itself, as other cell types have active mechanisms for releasing vimentin into the extracellular space (Figure 1). This especially includes neutrophils^[25,26] macrophages,^[27] and endothelial cells.^[28,29] While early studies have attributed extracellular vimentin to cytoskeletal debris and disruptions in the plasma membrane, it is now clear that it appears in the absence of cell damage.^[30] While the functions of cell surface vimentin are still largely mysterious, cell surface vimentin has been shown to act as a biochemical signal between different

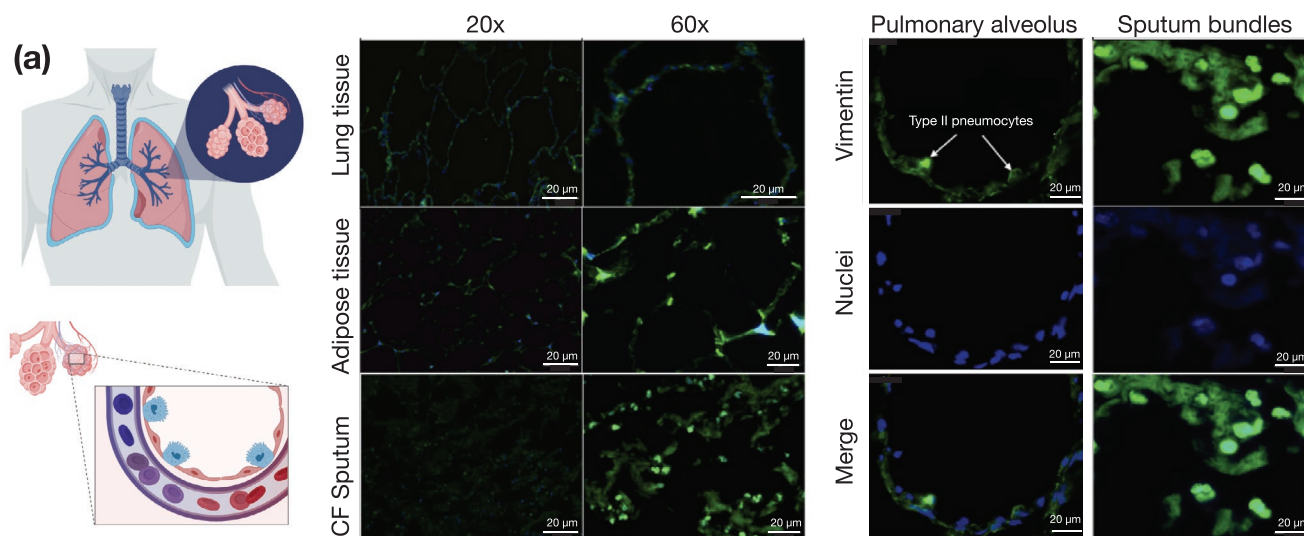
cell types but also serves as an attachment factor through which multiple types of bacteria and viruses infect cells.^[31,32]

The presence of vimentin on the surface of alveolar pneumocytes and in the extracellular space of the lungs was assessed with an anti-vimentin antibody by immunostaining healthy lung parenchyma without pathology and sputum samples collected from the respiratory tract of cystic fibrosis (CF) patients (Figure 1a). The presence of vimentin on the apical surface of type I and type II pneumocytes, cells without endogenous vimentin expression, indicates its extracellular origin. Immunostaining of airway sputum from CF patients showed the presence of vimentin in DNA-rich aggregate structures. Since obesity was identified as an important risk factor for complications in patients that suffered from SARS-CoV-2 infection,^[33] we also assessed the presence of vimentin in human adipose tissue (Figure 1a). Indeed, vimentin expression was present in the stromal tissue. The identification of extracellular vimentin in lung, sputum, and adipose tissue indicates a surprising pattern of extracellular vimentin presence in the interstitial tissue and its possible role in SARS-CoV-2 uptake in lung and other ACE2 expressing tissues.

2.2. Binding of Vimentin to the SARS-CoV-2 Spike Protein

Next, we tested whether vimentin could bind to SARS-CoV-2 pseudoviruses displaying the antigenically correct spike protein in vitro. These pseudoviruses present the SARS-CoV-2 spike protein on replication-incompetent virus particles that contain a heterologous lentiviral (HIV) core (Integral Molecular, RVP-701G). Binding of purified bacterially-expressed human vimentin to these pseudoviruses was measured by a combination of DLS and imaging by AFM. Figure 2A shows that the hydrodynamic radius of the pseudovirus was 60 nm, consistent with the expected size of a lentivirus similar to the size of SARS-CoV-2.^[46] As purified vimentin was added to the pseudovirus suspension, its hydrodynamic radius increases to approximately 150 nm. Here, the increase in apparent size is presumably due to the bridging together of pseudovirus by vimentin oligomers. We estimate that at the highest concentration of vimentin there is an excess of 6×10^4 vimentin oligomers to spike protein (Experimental Section). The increase in apparent size is not due to a separate contribution of large vimentin filaments to the mixture, because scattering from vimentin alone was negligible at all concentrations compared to that of the pseudovirus, and the increase in scattering of the mixtures is larger than the sum of separate contributions from pseudovirus and vimentin (Figure S1, Supporting Information). Separate measurement of the vimentin used for these studies showed that its effective hydrodynamic radius was approximately 75 nm, which represents a small oligomer of vimentin similar in size to those reported at the cell surface.^[47]

Vimentin is a strongly negatively-charged polyelectrolyte, which lends itself to strong counterion mediated interactions with other molecules.^[48] Thus, we next tested whether binding between the pseudovirus and vimentin was specific or a generic feature of polyelectrolytes. This was tested by using double-stranded DNA, which possesses a similar surface charge density to vimentin of approximately -0.5 nm^{-2} .^[48] Our DLS



(b) Pathways for vimentin expression in the lung and other tissue

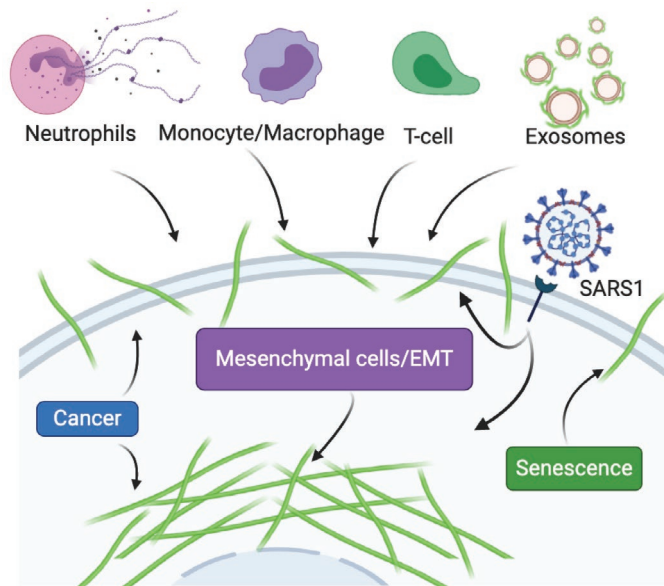


Figure 1. Presence of extracellular vimentin in human lung, airway fluids, and fat tissue. a) Positive staining for extracellular vimentin (green) in human lung, fat tissue, and sputum obtained from CF patients. Vimentin appears on the apical side of type I and type II pneumocytes. DNA stained with DAPI. b) There are numerous internal and exogenous pathways by which vimentin may be found in lung epithelia and other tissues, in either intracellular or cell surface forms (shown as green filaments). Vimentin is expressed directly by mesenchymal cells, cells having undergone EMT, cancer cells, senescent fibroblasts, and interestingly by cells bound and infected by the SARS-CoV virus (see Table 1). Exogenous sources of vimentin are largely related to immune response and tissue injury in the form of vimentin exported by neutrophils, T-lymphocytes, monocytes/macrophages, and exosomes. Created with BioRender.com.

measurements showed that the molecules were also of similar size, the hydrodynamic radius of vimentin being 75 nm and DNA, 115 nm. We found that the addition of double-stranded DNA did not lead to an increase in pseudovirus size (Figure S2, Supporting Information), suggesting binding of vimentin to the pseudoviruses is likely specific and not a result of the highly-charged polyelectrolyte nature of vimentin.

The samples used for DLS were also examined by AFM. Figure 2C shows the pseudovirus alone and pseudovirus after

the addition of DNA or vimentin. Histogram of the size distributions (Figure 2b) shows pseudovirus diameters consistent with the radii measured by DLS and that after addition of vimentin, some single pseudoviruses appear larger, but small clusters of pseudoviruses, possibly bridged by vimentin oligomers, are common. Binding of vimentin oligomers or short filaments to the pseudovirus was selective for vimentin; we found that similar increases in pseudovirus size after titration with three different preparations of vimentin, but no significant

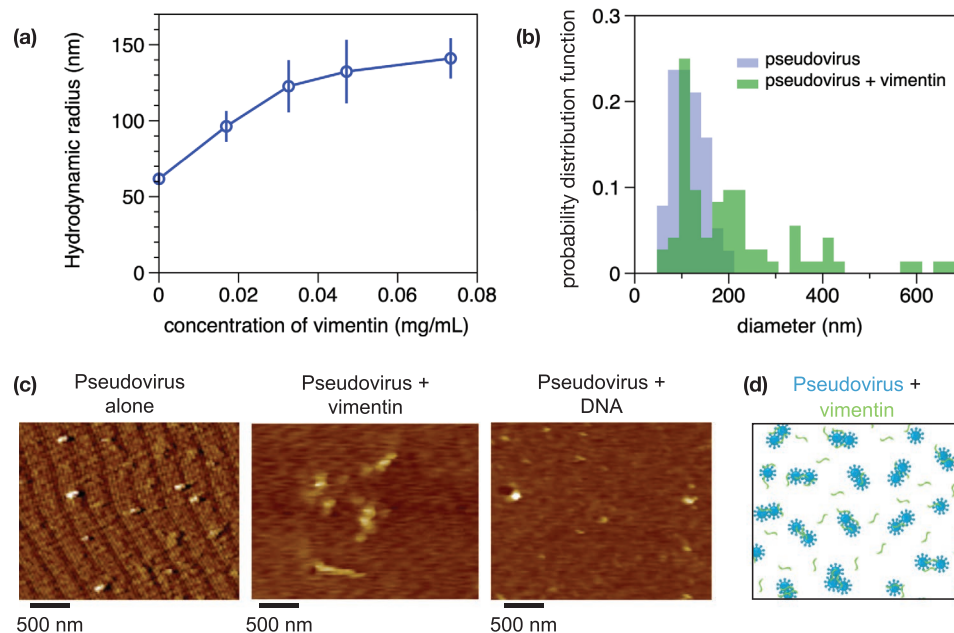


Figure 2. Binding of vimentin to SARS-CoV-2 pseudovirus. Purified human recombinant vimentin was added to suspensions of SARS-CoV-2 spike protein-containing pseudovirus, and their size was measured by a) DLS and b,c) AFM. The size of the pseudovirus as measured by DLS increased from 60 to 150 nm after the addition of 0.07 mg mL^{-1} vimentin (panel (a)). Panel (c): The pseudoviruses were imaged using AFM before and after the addition of either vimentin (0.07 mg mL^{-1}) or DNA (0.08 mg mL^{-1}). The probability distribution functions (b) show that the average size of pseudovirus imaged by AFM confirms the change in size detected by DLS. d) Schematic representation indicating how binding of vimentin to SARS-CoV-2 spike protein might couple particles together and increase their effective radii. Error bars denote standard deviation.

increase after the addition of double-stranded DNA, a polymer that is also found extracellularly with similar size and surface charge of vimentin (Figure S3, Supporting Information). Overall, the data in Figure 2 shows that purified vimentin can bind the SARS-CoV-2 spike protein-containing pseudoviruses and cause it to aggregate.

2.3. Anti-Vimentin Antibodies Block Uptake of SARS-CoV-2 Pseudoviruses in Cultured Human Epithelial Cell Lines

If extracellular vimentin can bind to SARS-CoV-2 virus and help capture it at the cell surface, then vimentin might increase SARS-CoV-2 host cell invasion by acting as an attachment factor, and anti-vimentin antibodies could block its uptake. To test this idea, we first examined whether external vimentin was present on the extracellular surface of mesenchymal cells such as fibroblasts and human embryonic kidney epithelial cells HEK 293T-hsACE2 (Figure 3), stably expressing the ACE2 receptor to enable host cell invasion by the SARS-CoV-2 pseudoviruses (Figure 3). To selectively label extracellular vimentin, we performed immunofluorescence studies in which live cells were first exposed to primary anti-vimentin antibodies (Novus Biologicals) for 1 h before being fixed with paraformaldehyde (see Experimental Section) and treated with secondary antibodies. In some cases, cells were then permeabilized and stained for F-actin with phalloidin to see cell shape. Figure 3 shows the immunofluorescent images of mouse embryonic fibroblasts (MEFs) and HEK-293T-hsACE2 cells stained with this novel technique to detect extracellular vimentin as well as traditional

immunofluorescence methods to show intracellular vimentin. As shown in Figure 3, vimentin was detected in both the cytoplasm (Figure 3a,c) and extracellular surface (Figure 3b,d) of the two different cell types. To map the distribution of vimentin in more detail, we imaged MEF cells stained for both intracellular and extracellular vimentin with super-resolution confocal microscopy (Figure 4; Experimental Section). Intracellular and extracellular vimentin possessed distinctly different immunofluorescence patterns in the two separate domains of the cell. Inside cells, the vimentin organized into filamentous bundles and networks, whereas the vimentin pattern was hazy and showed some localized clusters on the extracellular surface of the cell, consistent with prior reports.^[49,50]

Next, we performed host cell invasion studies using SARS-CoV-2 pseudoviruses bearing a green fluorescent protein (GFP) mRNA reporter (Figure 5). Cultured HEK 293T-hsACE2 were exposed to varying concentrations of pseudoviruses (Experimental Section), and the resulting number of transduced cells was detected by epifluorescence microscopy of cell GFP expression and monitored over the course of three days. As expected, the number of GFP-expressing cells increased over the course of three days, reaching maximum infection rates ranging from 1 to 10% among experimental replicates.

Can anti-vimentin antibodies block SARS-CoV-2 uptake and does inhibition depend on the antibody's vimentin-binding epitope? To address this question, we presented cells with a number of different antibodies against vimentin (see Table 1) and measured the resultant change in transduction compared to the case without antibodies. We began these studies with the most promising therapeutic anti-vimentin antibody,

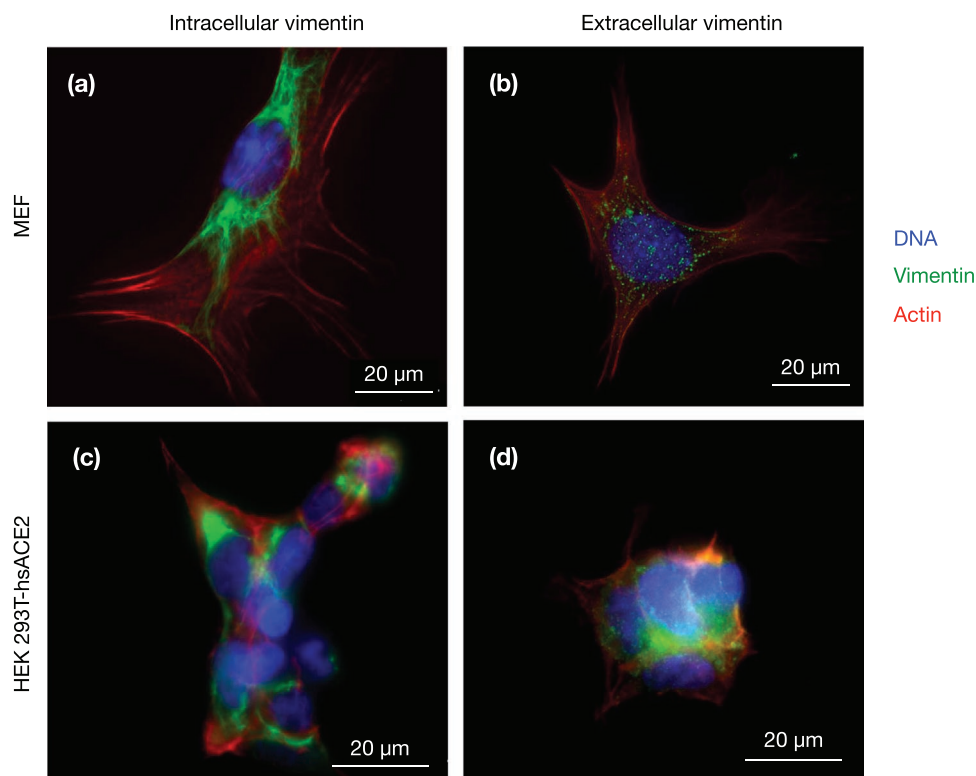


Figure 3. Intracellular and extracellular vimentin expression in MEF and HEK-293T-hsACE2. a,b) MEF stained for vimentin either (a) intracellularly with triton permeabilization before exposure to vimentin antibodies or (b) extracellularly, where cells were exposed to anti-vimentin antibodies before fixation, then permeabilized and stained for actin. Images show vimentin (green), actin (red), and DNA (blue). c,d) Positive staining for intracellular and extracellular vimentin was detected in human kidney epithelial cells HEK 293T-hs ACE2.

Pritumumab, a human-derived IgG antibody, reported to be specific against extracellular vimentin and known to bind to vimentin's C-terminal domain.^[51] In this case, we pre-exposed

HEK 293T-hsACE2 cells with various concentrations of Pritumumab prior to infection by SARS-CoV-2 pseudoviruses and found a dose-dependent decrease in infection efficiency

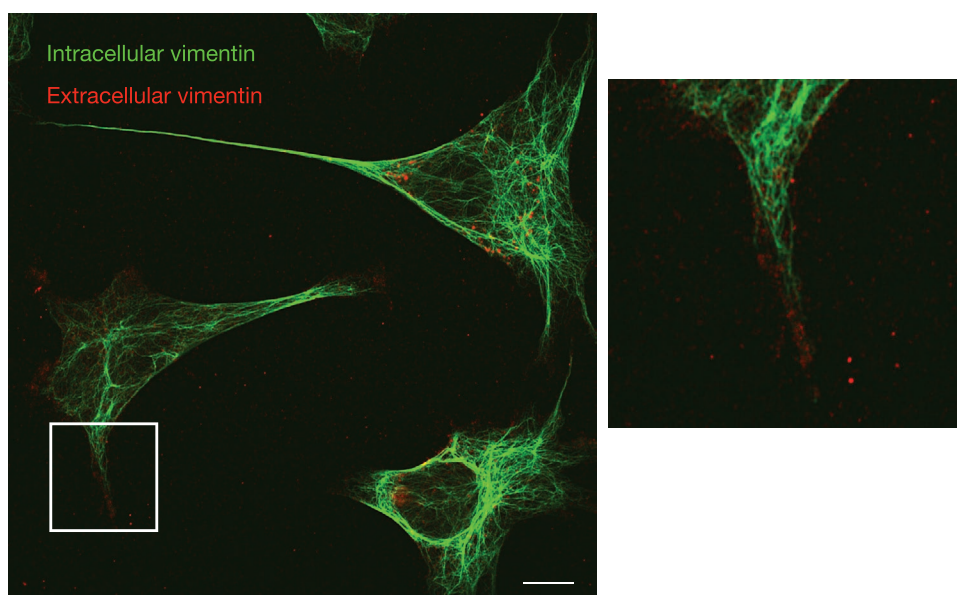


Figure 4. Distribution of intracellular and extracellular vimentin in MEF. Super-resolution confocal images showing MEF cells exposed first to a primary anti-vimentin antibody (human, Pritumumab) to bind to vimentin on the extracellular surface of the cells, then fixed, permeabilized, and exposed to a second primary anti-vimentin antibody (chicken, NOVUS) to bind to intracellular vimentin. This immunofluorescence technique reveals the two distinct organization patterns of intracellular cytoskeletal vimentin and extracellular vimentin. Scale bar; 10 µm.

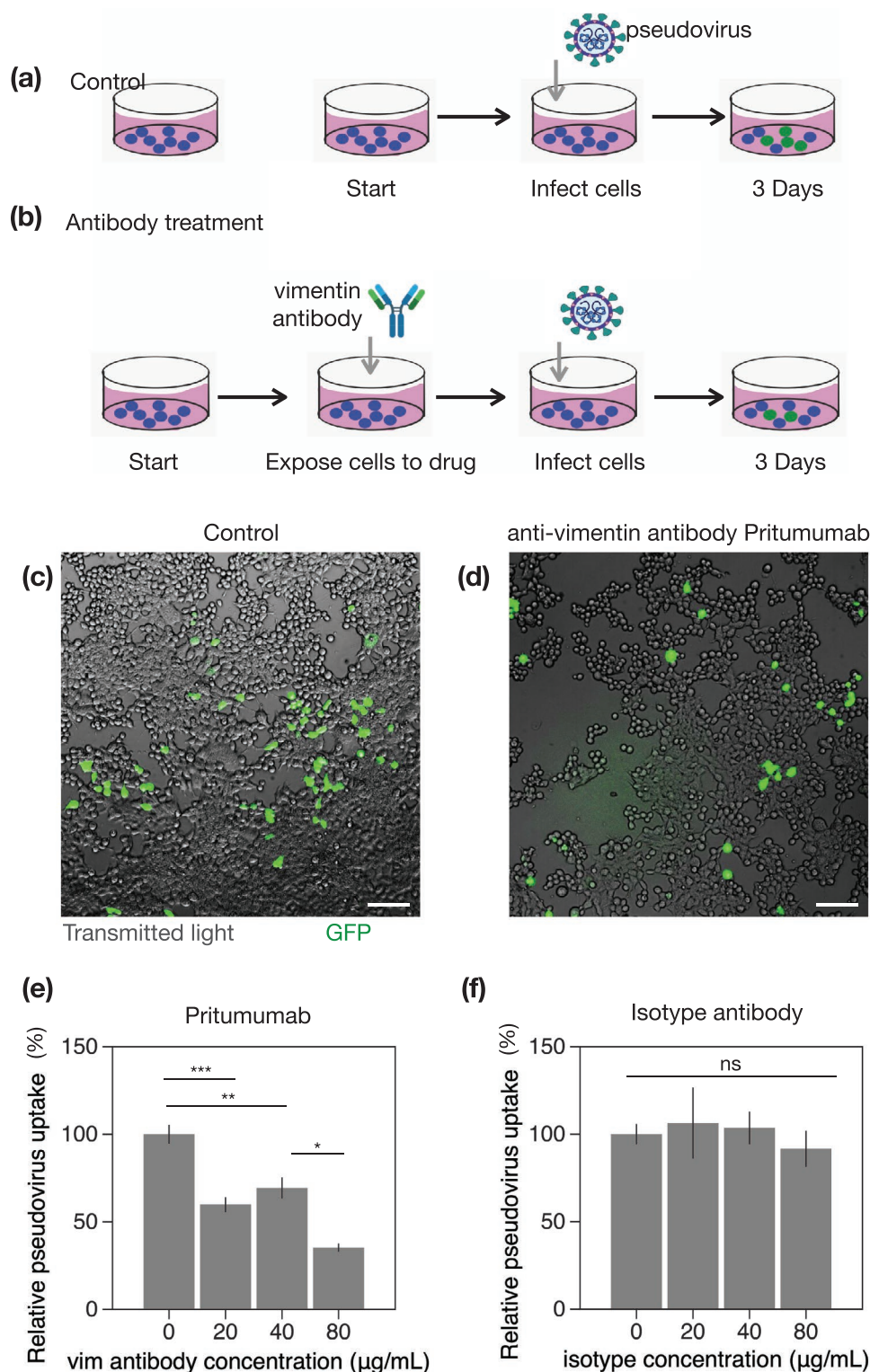


Figure 5. Anti-vimentin antibodies block uptake of Wuhan-Hu-1 SARS-CoV-2 pseudovirus in HEK 293T-hsACE2. a) HEK 293T-hsACE2 were exposed to pseudovirus particles bearing the SARS-CoV-2 spike protein and a GFP reporter. Cells were imaged three days after exposure to detect the number of cells expressing GFP, indicating the number of cells transfected by pseudoviruses. b) In the antibody treatment case, cells were pre-exposed to anti-vimentin antibodies before infection by the pseudovirus. c,d) Fluorescence images showing cells expressing GFP after pseudovirus exposure with and without Pritumumab treatment. Scale bar; 100 µm. e) Pritumumab inhibits cellular infection by up to 60%. f) Use of an isotype antibody does not inhibit infection, suggesting a specific interaction between the SARS-CoV-2 spike protein and extracellular vimentin. Error bars denote standard deviation. Denotations: * $P \leq 0.05$; ** $P < 0.01$; *** $P < 0.001$; NS, $P > 0.05$.

Table 1. Sources of intracellular and exported vimentin.

Source	Description	Reference
Extracellular Sources—Largely implicated in immune and tissue injury		
Neutrophils	Released during apoptosis or NET formation; Source of serum citrullinated vimentin commonly found in rheumatoid arthritis	[26,34]
Monocytes/ Macrophages	Secreted after stimulation by TNF- α or oxidized low density lipoprotein; possibly tissue injury; phosphorylated	[27,35]
T-lymphocytes	Released on apoptosis; Binds phospholipase II to promote arachidonic acid metabolism	[36]
Exosomes	Astrocytes, activated by injury, can produce extracellular vimentin in the form of exosomes that are delivered to neurons; pre-adipocytes	[37–39]
Sources from the cell itself—Mesenchymal and transformed cells		
Mesenchymal cells/EMT	Vimentin is expressed endogenously in mesenchymal cells and is a wide-spread marker EMT	[40,41]
Cancer	Intracellular: Upregulation of vimentin in multiple types of cancer; Extracellular: Target for isolating circulating tumor cells, designing vaccines and enhanced chemotherapy; sometimes proteolyzed	[42,43]
Senescent Fibroblasts	Post-translational modification of cysteine 328 by malondialdehyde in senescent cells leads to its secretion and surface exposure	[44]
SARS-CoV Stimulation	Extracellular vimentin expression increases upon SARS-CoV binding to cell surface; SARS-CoV also upregulates cytoplasmic vimentin by the TGF- β pathway to promote a fibrotic response in lung cells	[19,45]

(Figure 5). We found a 60% decrease in SARS-CoV-2 pseudovirus uptake at a Pritumumab concentration of 80 $\mu\text{g mL}^{-1}$. Uptake levels after treatment with 20 and 40 $\mu\text{g mL}^{-1}$ Pritumumab, were statistically similar under these conditions, reducing the uptake by approximately 40%, which suggests that lower concentrations of Pritumumab might still be therapeutically effective. The specificity of the Pritumumab interaction with extracellular vimentin was tested against an IgG isotype

Table 2. List of anti-vimentin antibodies.

	Anti-Vimentin antibody	Binding domain on vimentin	Effectiveness in blocking uptake of Wuhan-Hu-1 SARS-CoV-2 pseudovirus in HEK 293T-hsACE2
1	Pritumumab (Nascent Biotech); A natural human IgG1 kappa antibody was obtained from a regional draining lymph node of a patient with cervical carcinoma	Epitope is the C2 core region (coil 2 of the central rod) of cell-surface vimentin ^[51,52]	Blocks uptake up to 60% (Figure 5e)
2	Chicken polyclonal IgY antibody (Novus Biologicals)-Cat# NB300-223 (C-terminal/antigen whole molecule of purified human vimentin)	Polyclonal antibody, multiple epitopes	Blocks uptake up to 70% (Figure 6a)
3	Rabbit Recombinant Anti-Vimentin antibody-IgG $M_w \approx 150$ kDa [EPR3776] (Abcam) Cat# ab92547 (C-terminal)	C-terminal; produced by immunizing with a synthetic peptide containing 17 residues from within amino acids 425–466 of human vimentin	Blocks uptake up to 40% (Figure 6d)
4	Rabbit Monoclonal (Cell signaling Technology) Cat# 5741	N-terminal; produced by immunizing with a synthetic peptide corresponding to residues surrounding Arg45 of human vimentin	Does not block uptake (Figure S4a, Supporting Information)
5	Rabbit Primary anti-vimentin polyclonal antibody IgG ≈ 150 kDa (antibodies-online.com) Cat# ABIN6280132 (N-terminal)	N-terminal; Synthesized peptide derived from human Vimentin around the non-phosphorylated site of Ser56, Binding Specificity AA 1–80, Ser56	Does not block uptake (Figure S4b, Supporting Information)

antibody control (Figure 5d), which did not block entry of the SARS-CoV-2 pseudoviruses, suggesting a specific interaction between vimentin and the SARS-CoV-2 spike protein.

Next, we tested the efficiency of different anti-vimentin antibodies (Table 2) in blocking host cell invasion by pseudoviruses carrying spike proteins from the native Wuhan-Hu-1 strain and its variants UK B.1.1.7 and Brazil P.1 that have recently become commercially available (Experimental Section). As shown in Figure 6, both a chicken polyclonal anti-vimentin antibody that binds to multiple epitopes of the vimentin C-terminus (Figure 5a–c) and a rabbit anti-vimentin antibody targeting amino acids 425–466 of the vimentin C-terminus (Figure 6d–f) significantly decreased uptake of the Wuhan-Hu-1 pseudoviruses and the two other spike variants. Not all anti-vimentin antibodies effectively blocked SARS-CoV-2 pseudoviruses cellular uptake. In particular, we found that two vimentin antibodies targeting the vimentin N-terminus (a monoclonal rabbit antibody corresponding to residues surrounding Arg45 and a polyclonal rabbit antibody IgG around the non-phosphorylation site of Ser56) did not block uptake of Wuhan-Hu-1 pseudoviruses in HEK 293T-hsACE2 (Figure S4, Supporting Information). The higher effectiveness of antibodies targeting the C-terminal tail domain of vimentin suggests that the binding interface between the spike protein and vimentin is on the C-terminal half of the protein. Taken together, Figure 6 indicates that anti-vimentin antibodies inhibit the uptake of pseudoviruses decorated with the spike protein of the native Wuhan-Hu-1 strain and its variants UK B.1.1.7 and Brazil P.1, which suggests that anti-vimentin antibodies may be effective in blocking other novel SARS-CoV-2 mutants.

Our results thus far indicate that SARS-CoV-2 spike protein binds to vimentin on the extracellular surface of the cell, facilitating the delivery of the pseudovirus to the ACE2 receptor and increasing host cell invasion. This interaction can be targeted by exposing cells to anti-vimentin antibodies that bind to the cell surface vimentin and block vimentin's interaction with the SARS-CoV-2 spike protein. Assuming vimentin binds to the SARS-CoV-2 spike protein, then another approach to block SARS-CoV-2 pseudoviruses uptake is to neutralize the particles

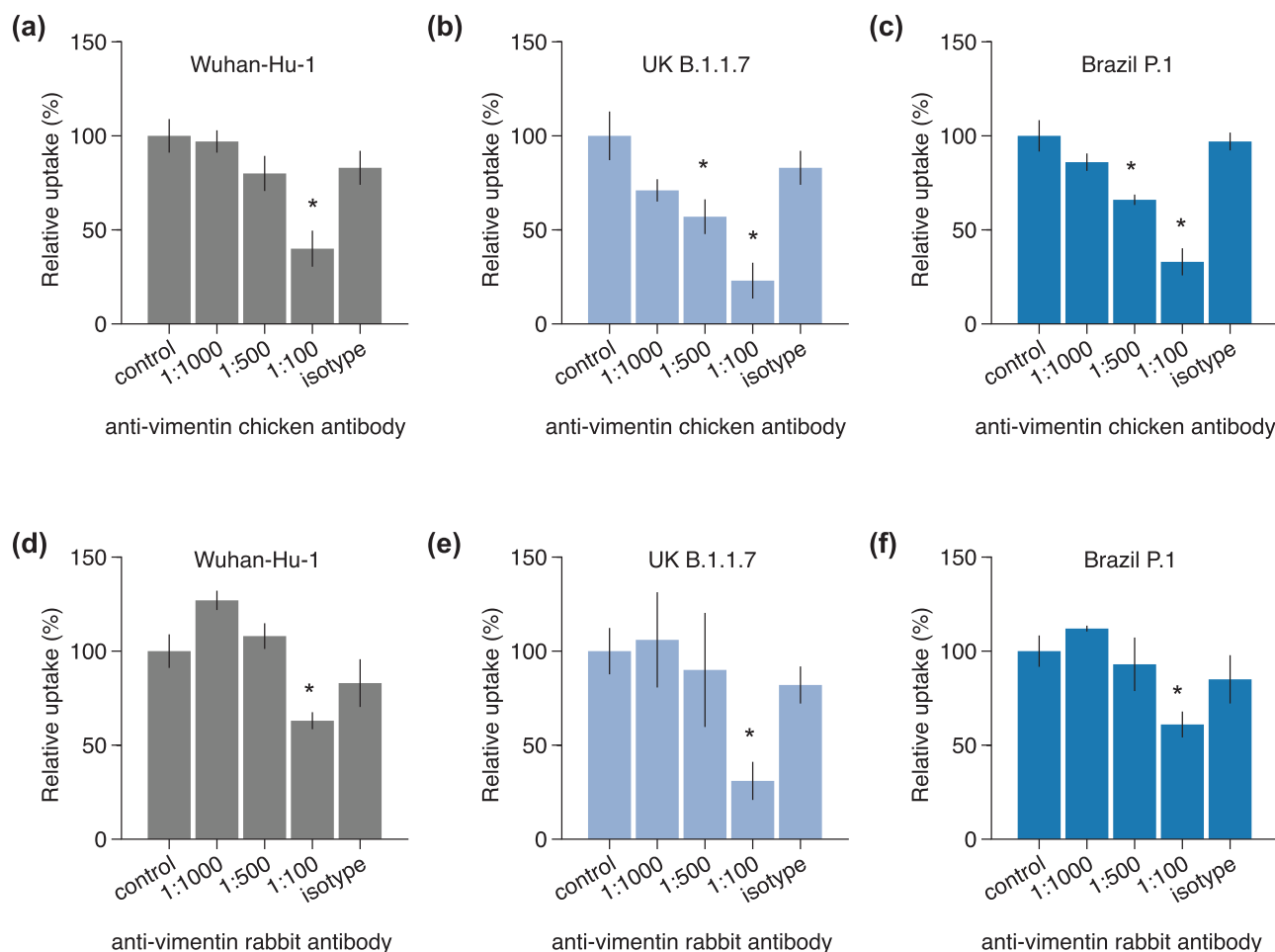


Figure 6. Effect of vimentin antibodies on cellular uptake of pseudoviruses bearing spike protein from three different strains of SARS-CoV-2. The effect of a–c) chicken polyclonal anti-vimentin antibodies (C-terminal, multiple epitopes) and d–f) rabbit monoclonal (against C-terminal 425–466) and their respective isotypes were tested in the uptake of pseudo-virus bearing spike proteins from three different strains: Wuhan-Hu-1, UK B.1.1.7, and Brazil P.1. Isotypes were diluted 1:100. Experiments were conducted in HEK 293T-hsACE2 and measured via plate readers (Experimental Section). Error bars denote standard deviation. Denotations: * $P \leq 0.05$.

by first exposing the pseudoviruses to soluble vimentin that binds to and sequesters the spike proteins on the pseudovirus.^[12,49,53] Here we tested the effectiveness of recombinant human vimentin (NOVUS Biological) in blocking uptake of the SARS-CoV-2 pseudoviruses by preincubating vimentin with the pseudoviruses before their exposure to the HEK 293T-hsACE2 cells. Our results show (Figure 7) that the addition of either 0.01 or 0.05 mg mL⁻¹ vimentin blocks approximately 50% of the uptake of pseudoviruses bearing the native Wuhan-Hu-1 spike protein and the UK B.1.1.7 variant, but was not effective in blocking uptake in the Brazil P.1 variant. The results in Figure 7 suggest that soluble vimentin is capable of blocking SARS-CoV-2 pseudoviral entry but the technique is not as effective as anti-vimentin antibodies (Figure 6). These variable results are consistent with prior studies, which have shown that soluble vimentin can inhibit viral entry^[12] but also in some cases enhance it.^[49] The precise effects of soluble vimentin on viral uptake are unclear, but it is thought that soluble vimentin may have two competing effects that regulate total viral uptake. The first is that vimentin binds to and deactivates the spike protein on the virus; the second is that vimentin may also adsorb on the

cell surface, which would help facilitate delivery of a vimentin-coated virus to the cell surface.^[49] The total effect of soluble vimentin may thus increase or decrease virus uptake depending on the details of binding between vimentin and the cell surface and the competition of available binding sites between the spike protein, vimentin, and cell surface receptors (e.g., ACE2). Circulating levels of vimentin in serum of patients with coronary artery disease, a condition that increases extracellular vimentin are less than 0.2 $\mu\text{g mL}^{-1}$.^[54] Frescas et al.^[44] show in a mouse model that plasma vimentin can be as much as 6 $\mu\text{g mL}^{-1}$. This is below the concentration needed for half-maximal change in DLS (Figure 2A) though perhaps still within the range where it might be relevant in vivo.

2.4. Cell Surface Vimentin Acquisition from the Extracellular Environment

Our results thus far suggest that cell surface vimentin on the extracellular surface of the cell binds to the SARS-CoV-2 spike protein and enhances host cell invasion by SARS-CoV-2.

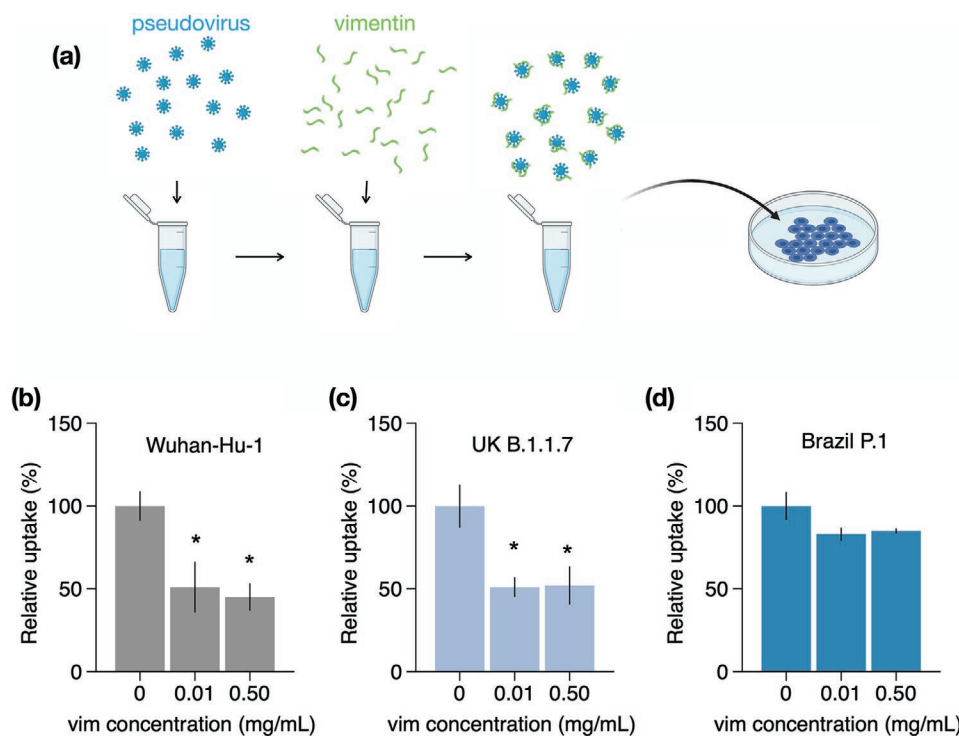


Figure 7. Effect of soluble vimentin on SARS-CoV-2 pseudovirus uptake in HEK293T hsACE2. The effect of vimentin itself on SARS-CoV-2 pseudovirus uptake was assessed by pre-exposing pseudoviruses with recombinant human vimentin (NOVUS Biological) for 20 min before their addition to HEK 293T-hsACE2 cells. a) Schematic of vimentin neutralization experiment. Vimentin blocked approximately 50% of uptake in b) the native Wuhan-Hu-1 strain and c) the UK B.1.1.7 variant, but did not block uptake in d) the Brazil P.1. variant. Error bars denote standard deviation. Denotations: * $P \leq 0.05$.

Studies on SARS-CoV and SARS-CoV-2 indicate that while ACE2 is required for infection, it is not solely sufficient for cellular uptake and invasion.^[7] We therefore posit that extracellular vimentin is a key player in SARS-CoV-2 invasion and that its presence in the lung and other tissues is an important pre-condition of the extracellular environment that enhances SARS-CoV-2 infection. As a pre-requisite, we have identified that vimentin is present in extracellular space of healthy adult lung and fat tissue (Figure 1). Vimentin may appear on the cell surface and in the extracellular space of the lung via numerous routes (Figure 1, Table 1). These routes are likely associated with an inflammatory response in the course of disease (e.g., fibrosis and cancer) but might also reflect homeostatic regulation associated with normal tissue functions and maintenance. In the context of the lung, the most probable sources are vimentin-expressing lymphocytes, macrophages, and neutrophils that specialize in fighting off pathogens.

Here, we demonstrate a novel mechanism by which non-vimentin expressing cells acquire cell surface vimentin from the extracellular environment via neutrophil NETosis.^[25,34] NETosis represents one of the mechanisms of host defense, in which neutrophils expel large webs of DNA that entrap bacteria in neutrophil extracellular traps (NETs). Additionally, during NETosis disassembly of the vimentin network takes place. NETosis requires activation of peptidyl arginine deiminase 4 (PAD4), which citrullinates histones in the process of releasing DNA from neutrophil heterochromatin. At the same time, the cytoskeleton disassembles to allow the nuclear content released after nuclear membrane rupture to reach the plasma

membrane and eventually enter the extracellular space as the plasma membrane ruptures.^[34] Disassembly of the vimentin network is also promoted by citrullination, and vimentin is a major substrate for PADs.^[25] Citrullination leads to the disassembly of the vimentin network, which can then be released into the extracellular space and become accessible to the cell surfaces of other tissues.

We designed an experiment to test whether neutrophil-released vimentin can be acquired on the surface of other cell types (Figure 8a). First, we stimulated NETosis in a suspension of neutrophils with phorbol myristate acetate (PMA), which induces disassembly of the cytoskeleton and release of DNA and vimentin into the extracellular ambient fluid.^[25,34] Next, we centrifuged the neutrophil suspension and collected the supernatant, which we posited contained soluble vimentin released from the neutrophils during NETosis. To identify if there was soluble vimentin in the supernatant and whether this vimentin could be captured and presented on surfaces of other cell types, the neutrophil-harvested supernatant was added to a prewashed dish of vimentin-null MEF. After exposure, the vimentin-null MEF were fixed and stained using anti-vimentin antibodies (Figure 8b). Since vimentin-null MEFs were used, any vimentin detected on their surface was indicative of vimentin acquired from the extracellular environment. As shown in Figure 8b, after exposing cells to the neutrophil supernatant, the vimentin-null cells stained positive for cell-surface vimentin in immunofluorescence microscopy. These results indicate a mechanism by which vimentin is released into the extracellular environment of tissues, where it can then bind to the extracellular

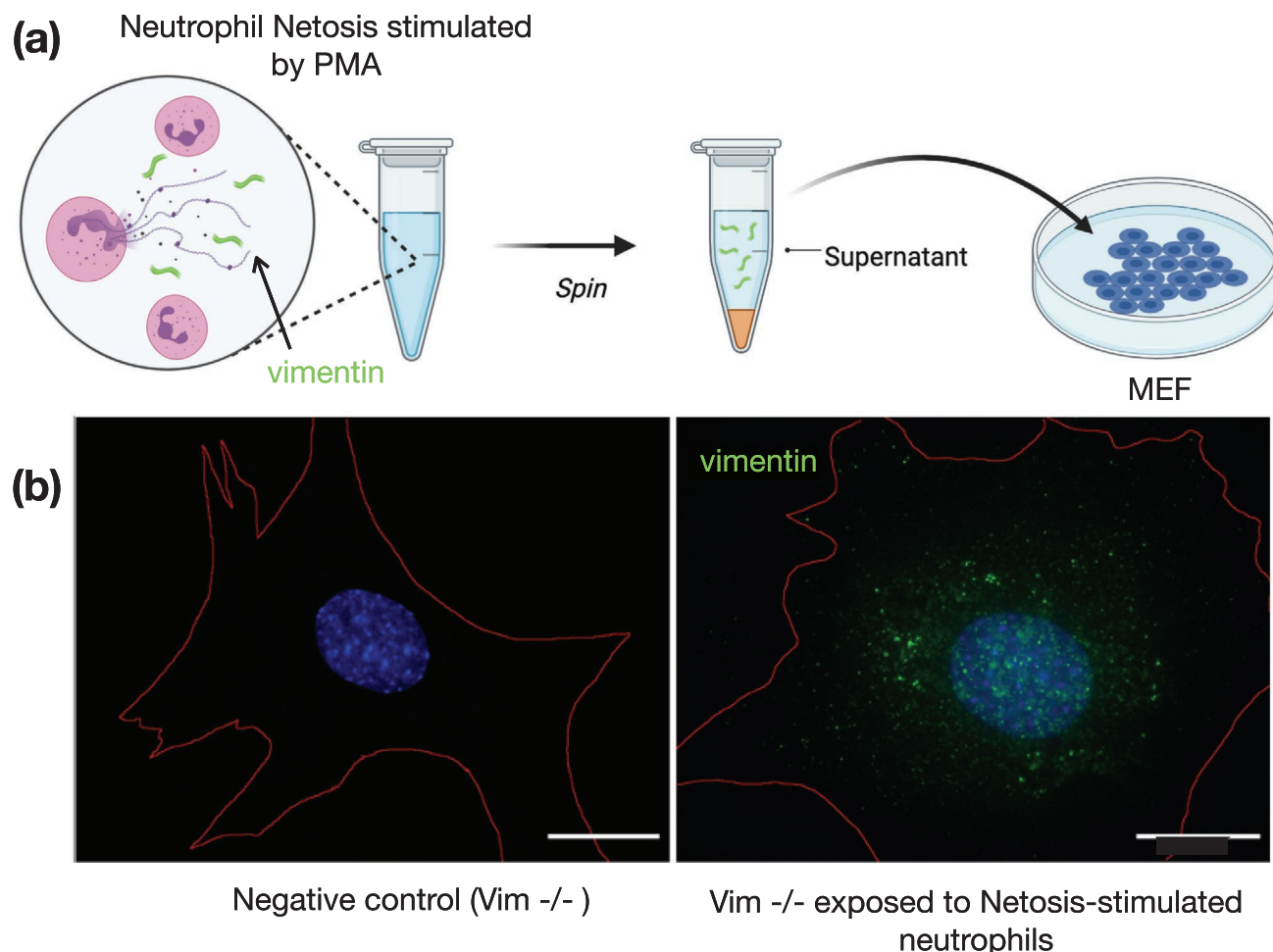


Figure 8. Acquisition of cell surface vimentin from the extracellular environment. a) To determine whether vimentin released from neutrophil NETosis could be acquired on the surface of other cell types, we stimulated neutrophil NETosis with PMA, centrifuged, and collected the supernatant. The neutrophil-stimulated supernatant was then presented to vimentin-null (*vim*^{-/-}) MEF, which were subsequently fixed and stained to detect acquired vimentin. b) Immunofluorescence images of vimentin-null MEF staining positive for extracellular vimentin after exposure to supernatant of NETosis-activated neutrophils, indicating the acquisition of extracellular vimentin by cells that do not express vimentin. Cell boundary is marked in red. Scale bar, 20 μ m. Created with BioRender.com.

surface of cells. Treatment of cells with DNase did not prevent vimentin deposition on cells (Figure S5, Supporting Information), indicating that vimentin was not binding to the cell surface through DNA, which is also released upon NETosis.

Because soluble vimentin binds the surface of SARS-CoV-2, it is possible that antivimentin antibodies might also function to bind and aggregate vimentin-coated viruses, thereby inhibiting their infectivity and facilitating their clearance. We tested for this mechanism by light scattering studies to determine if adding anti-vimentin to SARS-CoV-2 pseudoviruses after their exposure to vimentin further increased scattering as expected if aggregates formed. Figure S6, Supporting Information, shows that the scattering intensity of a suspension of pseudoviruses is increased by the addition of soluble vimentin oligomers, consistent with the results in Figure 2a, but the addition of an anti-vimentin antibody has no additional effect on the scattering intensity (Figure S6, Supporting Information). These results suggest that at least the chicken vimentin antibody, which is effective in preventing infection of cells by

SARS-CoV-2, does not act by aggregating vimentin-coated viral particles into large complexes that might be cleared or otherwise prevented from infecting the host cell. Figure S6, Supporting Information, also shows that the addition of the anti-vimentin antibody to the pseudoviruses without vimentin has no effect on the scattering intensity. Therefore although we cannot rule out an effect of soluble vimentin on SARS-CoV before it reaches a cell surface, our results show that aggregation of the virus by a combination of vimentin and anti-vimentin antibodies prior to their binding the host cell does not account for the ability of these antibodies to inhibit infection.

2.5. Modeling the Interactions between Cell Surface Vimentin and SARS-CoV-2

Both SARS-CoV and SARS-CoV-2 can enter host cells via both membrane fusion and endocytic pathways; although both

pathways are dependent upon ACE2 binding.^[55–60] Emerging evidence indicates that membrane fusion is the dominant pathway when the transmembrane protease serine 2 TMPRSS2 is present on the cell surface.^[61] However, in the absence of such proteases, coronaviruses will use clathrin- and non-clathrin-mediated endocytosis.^[57,62] TMPRSS is expressed in lung cells,^[63,64] but during later stages of SARS-CoV-2 infection, the virus spreads to different tissues and infects other cell types.^[65,66] As extracellular vimentin binds to the SARS-CoV-2 spike protein (Figure 2), then extracellular vimentin could help adhere the virus to the cell surface and mediate cell membrane dynamics at scales relevant to fusion and endocytosis.

To provide an interpretive framework for our results (Figures 5 and 6), we developed a new 3D computational model of SARS-CoV-2, the cell membrane, and extracellular vimentin (Figure 9). In this picture, vimentin is treated as a co-receptor of the virus with an effective binding affinity less than the virus and ACE2. While the binding site between the SARS-CoV-2 spike protein and vimentin is thought to be on the C-terminal domain of vimentin, cell surface vimentin is in the form of 4–12 tetramers.^[47] Thus, each cell surface vimentin structure has multiple sites of potential binding to the spike protein. Given the atomistic complexity of vimentin, combined with the need to explore lengths on the scale of the entire virus and time

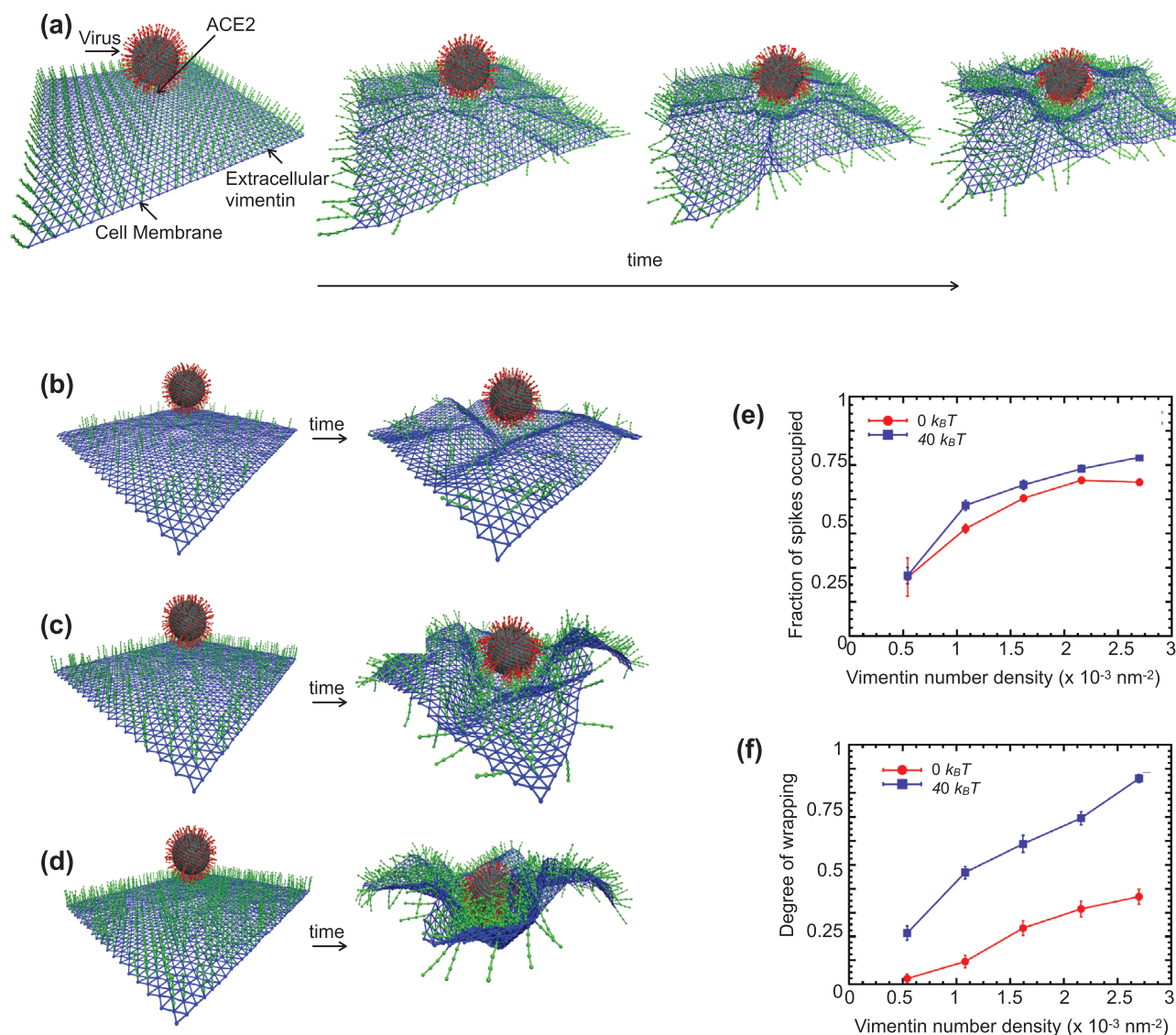


Figure 9. Vimentin's involvement in spike-ACE2 interactions. a) Cell surface vimentin acts as a co-receptor that enhances binding to the SARS-CoV-2 virus in either direct fusion or endocytic pathways to enhance wrapping and endocytosis of the virus. A molecular dynamics simulation of the SARS-CoV-2 virus attached to a cell membrane shows that binding of extracellular vimentin with the virus spike protein facilitates wrapping of cell membrane around the virus. Snapshots are shown at $t = 0, 170, 330,$ and 500 ms . b–d) Representative snapshots of simulations with cell surface vimentin densities of (b) 0.5×10^{-3} , (c) 1.6×10^{-3} , and (d) $2.7 \times 10^{-3} \text{ nm}^{-2}$. First ($t = 0 \text{ ms}$) and final frame ($t = 500 \text{ ms}$) are shown. Both the e) fraction of spikes bound to surface vimentin and the f) degree of membrane wrapping increases as the number density of surface vimentin increases. Finite membrane bending rigidity ($40 \text{ k}_B T$, blue squares) enhances wrapping compared to the case without bending rigidity ($0 \text{ k}_B T$, red circles).

scales relevant to membrane wrapping, we treat binding interactions between vimentin and the spike protein in a coarse-grained manner, averaging over many molecular interactions, by using an effective attractive interaction, as detailed in the Supporting Information. Specifically, cell surface vimentin is treated as a semiflexible filament, 40 nm in length, and the virus is a 50 nm radius sphere with 200 spikes. Two hundred spikes are chosen as an upper estimate on the number of spike proteins observed in SARS-CoV-2.^[67] The cell membrane is modeled as a thermally-fluctuating elastic sheet, which is either purely elastic with no bending rigidity ($0 k_B T$) or elastic with finite membrane rigidity ($40 k_B T$). The simulation begins with the virus attached to the cell membrane via an ACE2 binding site. For modeling details, see Experimental Section and Supporting Information materials.

As shown in Figure 9, we find that these simple interaction rules drive the cell membrane to partially wrap around the virus and in effect allow the virus to interact with an increased surface area of the cell membrane. Increasing cell-surface vimentin increases the fraction of spikes bound to cell surface vimentin and increases the effective degree of wrapping around the cell virus (Experimental Section). Interestingly, finite cell membrane bending rigidity enhances wrapping of the virus, as compared to the case where the cell membrane is elastic in stretch and compression alone. These results presented in Figure 9 indicate that co-receptors, such as cell surface vimentin, increase the effective interactions between the SARS-CoV-2 virus and the cell membrane. In acting as an attachment factor, cell surface vimentin would enhance the probability of a viral fusion event and could perhaps stimulate cell membrane wrapping around the virus (Figure 9), initiating the first steps towards viral endocytosis.

3. Discussion

Identifying targets against SARS-CoV-2 is critical because evidence suggests that viral load is correlated to the severity of COVID-19 infection in patients.^[68] Here, we have shown that extracellular vimentin promotes SARS-CoV-2 uptake in lung and kidney epithelial cells and antibodies targeted against vimentin block it. Thus, we propose that vimentin-blocking antibodies could serve as a promising therapeutic strategy against SARS-CoV-2 and future coronaviruses, decreasing viral load, and subsequent patient symptoms.

Although generally considered primarily an intracellular, cytoskeleton protein, a large body of evidence shows that vimentin can also be found on the external surface of cells and in extracellular fluids. Numerous pathways have been identified for controlled release of vimentin often by inflammatory cells. Extracellular release depends on covalent modifications of vimentin, often by phosphorylation or citrullination.^[30] These modifications disassemble cytoskeletal vimentin IFs and lead to the release of vimentin either on the external surface of the same cell or in soluble form or on the surface of exosomes where it can target cells such as epithelial cells^[69] or neurons^[38,39] that do not express vimentin endogenously. Cell surface vimentin is reported to function normally during some types of wound healing^[39,69,70] but is also often increased

during pathological states such as cancer^[71,72] and has been shown to increase motility in different breast and lung cancer cell lines.^[53,73] Numerous pathogens, both viruses and bacteria, exploit cell surface vimentin to gain entry to the host cell.^[11–19] In bacteria, engagement of vimentin can be due to the binding of essential virulence factors.^[74] For viruses that are affected by vimentin, binding depends on coat proteins, and in case of SARS-CoV, the binding molecule for vimentin is its spike protein, which is similar to the spike proteins of SARS-CoV-2.^[19]

The data presented here suggest that extracellular vimentin serves as a co-receptor of SARS-CoV-2, and new studies are beginning to investigate the molecular interactions between vimentin and the SARS-CoV-2 spike protein. Recently, Lam, Brown, and Ronca^[75] found that the affinity between the recombinant rod domain of vimentin and the spike protein quantified by its dissociation constant is 180 nM, which is a weaker binding affinity than the reported 15–120 nM^[1,76] range for SARS-CoV-2 spike-ACE2 affinity. Interestingly a recent study by Lalioti et al. has shown the SARS-CoV-2 spike protein colocalizes with extracellular vimentin, though to an extent that depends on cell type.^[50] Together, these data indicate that vimentin is capable of binding to the virus, and this initial engagement with the virus at the surface of the cell may help deliver the virus to the ACE2 receptor and ultimately enhance viral uptake. Figures 5 and 6 indicate that anti-vimentin antibodies block this molecular interaction to inhibit viral uptake, as schematically illustrated in Figure 10.

From a physiological perspective, the ability of cells to acquire vimentin molecules released from activated neutrophils or damaged cells suggests that most of the released vimentin is attached to the cell surface in contrast to being soluble and in the bloodstream. We therefore hypothesize that at infection

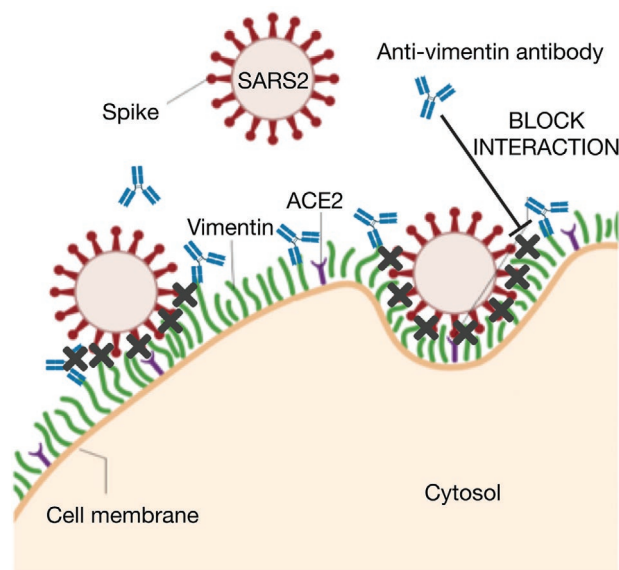


Figure 10. Extracellular vimentin as a potential target for inhibiting SARS-CoV-2 entry. A diagram of the proposed mechanism of action. Here, cell surface vimentin (green) acts as a co-receptor that binds to SARS-CoV-2 spike protein. Blocking this interaction by anti-vimentin antibodies reduces cell surface binding of the virus and cellular infection. Created with BioRender.com.

sites vimentin released from immunocompetent cells mostly serves mainly as co-receptor for virus entry upon its binding to the cells that served as a virions' target. This effect however may be context-dependent. In cases where there might be high levels of soluble vimentin that may sequester virions from entry receptors or too much cell-surface vimentin that may trap and hinder the virus, then vimentin may act to decrease infection.

While these studies focus on extracellular vimentin and the critical first steps by which SARS-CoV-2 pseudo-particles bind and invade cells, new *in vivo* studies are also emerging. In the Lam, Brown, and Ronca study, recombinant vimentin blocked the uptake of the live SARS-CoV-2 virus in Vero cells,^[75] and a study by Li et al. has shown that small molecule vimentin inhibitors improve the outcome after infection in a Mouse-Adapted SARS-CoV2 model.^[77] Both monoclonal anti-vimentin antibodies and a vimentin-specific DNA aptamer developed to isolate circulating cancer cells^[78] are being applied to infection by SARS-CoV^[19] and other viruses.^[79] Much further work is needed to understand vimentin's role in viral infection, but our results and those of others^[50,53,75,77] point to a largely unrecognized target—extracellular vimentin—as a novel therapeutic target against host cell invasion by SARS-CoV-2 and other viruses.

4. Conclusions

Vimentin is secreted into the extracellular environment by multiple cell types, and its presence can provide positive signals for wound healing and act as a cofactor for pathogen infection. Here, we have demonstrated a new role of extracellular vimentin in SARS-CoV-2 host cell invasion. Further, we find that antibodies against vimentin can block up to 80% of host cell invasion *in vitro*. Our results suggest a new target and therapeutic strategy to reduce SARS-CoV-2 attachment and entry into the cell, which could reduce the spread of the SARS-CoV-2 virus and other possible pathogens that exploit extracellular vimentin.

5. Experimental Section

Cell Culture: In this study, three cell lines were used: wild-type mouse embryonic fibroblasts (mEF vim +/+), vimentin-null fibroblast (mEF vim -/-), and human kidney epithelial cells HEK293T ACE2-transfected (Integral Molecular, Integral Cat# C-HA101). Cells were cultured in DMEM (ATCC) with 10% of fetal bovine serum (FBS), penicillin (50 µg mL⁻¹), and streptomycin (50 µg mL⁻¹). Kidney-derived cells were additionally treated with 0.5 µg mL⁻¹ puromycin to maintain ACE2 expression. Cells were maintained at 37 °C in an atmosphere containing 5% CO₂ with saturated humidity.

Tissue Staining: To evaluate the presence of extracellular vimentin on the surface of cells within human tissue, fluorescent immunohistochemistry staining was performed. To do so, paraffin-embedded human lung and fat tissue, as well as sputum obtained from CF patients were cut into 15 µm thick slices on a rotary microtome and placed on glass slides. After overnight drying, slides were immersed in xylene and ethanol for 10 min at each step. Slides were hydrated with PBS and transferred to EDTA-containing antigen retrieval solution (Sigma) for 1h at 100 °C. Subsequently, samples were blocked in blocking buffer (1% BSA in PBS) for 30 min at RT. Primary rabbit anti-vimentin antibodies to the C-terminus at 1:200 were placed directly on tissues and left for overnight incubation in a humidified chamber

at 4 °C. Afterwards, slides were washed three times for 15 min in PBS and incubated with secondary anti-rabbit Alexa Fluor 488-conjugated antibody at 1:500 for 1h at RT, protected from light. Following the washing step, tissues were counterstained with DAPI and mounted with anti-fade mounting medium (Sigma). Visualization was performed on a Leica DM2000 fluorescent microscope. The study involving human subjects was performed under protocols: APK.002.234.2021 and APK.002.235.2021 approved by the institutional review board (IRB) of The Medical University of Bialystok. The study was in accordance with the Declaration of Helsinki and written informed consent was provided by all subjects involved.

Dynamic Light Scattering: In these studies, recombinant human vimentin was kindly provided by Josef Käs and Jörg Schnauss (University of Leipzig) and by Karen Ridge (Northwestern Univ). The pseudovirus size (hydrodynamic radius) was determined by DLS using a DynaPro 99 instrument.^[80] The method measures the diffusion constant of the particles using the autocorrelation function of fluctuations in scattered light intensity. The radius R_h was calculated from the relation $D = k_B T / 6 \pi \mu R_h$, where D is the translational diffusion constant, k_B is the Boltzmann constant, T is the temperature, and μ is the solvent viscosity. To examine the interaction between the SARS-CoV-2 pseudovirus and vimentin, DLS measurements were performed on pseudovirus solutions with and without the addition of human recombinant vimentin. As a control for non-specific binding, in some cases, the addition of DNA was used to determine how polyelectrolyte polymers other than vimentin interact with the pseudoviruses. Interaction of spike protein incorporated into the pseudovirus's surface with vimentin oligomers would increase R_h either by adding to the surface of a single pseudovirus or by aggregation of viruses.

An estimate of the stoichiometry of vimentin oligomers to spike proteins was made from the concentration of pseudoviruses given by the manufacturer as 1.1×10^6 mL⁻¹, and the weight concentration and size of vimentin oligomers. Estimating the vimentin oligomer length as the hydrodynamic diameter, and the length of a vimentin unit length filament as 65 nm, led to an estimate of 3×10^{12} vimentin oligomers mL⁻¹ at the highest concentration. Assuming each pseudovirus contains 50 spike proteins led to an estimate of 5×10^7 spike proteins mL⁻¹. Therefore, at the highest concentration in the titration, there was a 6×10^4 excess of vimentin oligomers to spike protein.

Atomic Force Microscopy: A Multimode AFM with a Nanoscope IIIa controller (Veeco, Santa Barbara, CA) operated in contact mode was used to image pseudoviruses before and after the addition of vimentin or DNA. The cantilevers used were silicon nitride with a spring constant of 0.35 N m⁻¹ (Veeco, Santa Barbara, CA). The AFM was calibrated using a 3D reference of 200 nm height and 10 µm pitch (Digital Instruments, Santa Barbara, CA). Deflection and height images were obtained with scan rates of 1 Hz with a resolution of 512 pixels/line. Briefly, for AFM evaluation of pseudoviruses in control (non-vimentin addition) and samples preincubated with human recombinant vimentin, a 10 µL drop of pseudoviruses or pseudoviruses/vimentin was applied on cleaved mica (SPI Supplies, West Chester, PA) and analyzed in a dried environment.

Immunostaining of Cell Surface Vimentin: To visualize surface vimentin, cells were first exposed to a primary anti-vimentin antibody for 1 h. Primary antibodies for immunostaining included the Novus Biological chicken antibody or Pritumumab. Cells were then fixed in 4% paraformaldehyde for 30 min at 37 °C and stained with the secondary antibody, either anti-chicken Alexa Fluor 488 or anti-human Alexa Fluor 488, as appropriate. Counterstain was performed with DAPI nuclear stain. In some cases, cells were permeabilized with 0.1% Triton X-100 in PBS for 15 min after fixation and stained with either phalloidin to label F-actin or a second anti-vimentin antibody to label intracellular vimentin. Images were captured with a fixed-stage Zeiss Axio Examiner Z.1 microscope (Carl Zeiss Microscopy GmbH, Germany) and a confocal scanning unit (Yokogawa CSU-X1, Yokogawa Electric Corporation, Japan). Super-resolution images were captured using a Zeiss LSM 980 (Carl Zeiss, Germany) confocal microscope with Airyscan 2. The Zeiss 980 was equipped with a T-PMT, MA-PMTs, a GaAsP detector, and Airyscan 2 with

multiplex modes 4Y and 8Y. Optics used were a PI APO 63x/1.4 NA oil DIC. Zeiss Zen Blue 3.2 and 3.3 were used to capture the images.

Antibodies: For fluorescence imaging of vimentin and for experiments using anti-vimentin antibodies to block host cell transduction by SARS-CoV-2 pseudovirus, the following anti-vimentin antibodies were used: i) Pritumumab (Nascent Biotech), a human-derived IgG antibody that targets the C-terminus of vimentin; ii) Chicken polyclonal IgY antibody (Novus Biologicals, Cat# NB300-223); iii) primary anti-vimentin monoclonal antibody developed in rabbit immunized with a 17-residue synthetic peptide from a region within human vimentin amino acids 425–466 (Abcam, Cat# ab92547); iv) Rabbit Monoclonal (Cell signaling Technology, Cat#5741); and v) Ser56 N-terminus aa 1–80 (primary anti-vimentin polyclonal rabbit antibody; antibodies-online.com, Cat# ABIN6280132).

Pseudovirus Description and Manufacture: The pseudo-viruses used in these studies were SARS-CoV-2 GFP-reporter pseudovirus from Integral Molecular (Integral Cat# Wuhan-Hu-1RVP-701G, UK variant B.1.1.7 RVP-706G, and Brazilian variant P.1 RVP-708G). These pseudoviruses displayed antigenically correct spike protein pseudotyped on replication-incompetent virus particles that contain an HIV core. They were produced in HEK-293T cells using three separate plasmids, encoding the spike protein, a lentiviral gag polyprotein, and a reporter gene.

In Vitro Transduction of Cells by Pseudoviruses: HEK 293T-ACE2 cell lines were used as infection hosts for SARS-CoV-2 GFP-reporter pseudovirus (Integral Molecular, Integral Cat# RVP-701G). These SARS-CoV-2 pseudoviruses do not efficiently infect HEK 293T cells, thus HEK 293T-ACE2 was used, stably expressing the ACE2 receptor to enable host cell invasion. To transduce cells with the pseudovirus, cells were seeded in 96-well plates at approximately 50% confluency and pseudoviruses were introduced to cells by pipetting 50 μL (at 10^6 pseudoviruses mL^{-1}) into each well and in some cases by a serial 1/2 dilution of the pseudovirus. To assess the involvement of vimentin during SARS-CoV-2 infection, anti-vimentin antibodies were introduced into the wells either at the same time as the pseudovirus or for a short incubation time prior to pseudovirus exposure. The pseudoviruses were either washed out after a 2 h exposure time interval or were allowed to incubate with the cells throughout the remainder of the experiment. Cells were incubated for 72h at 37 °C with 5% CO_2 .

Pseudovirus Entry Characterization: Pseudovirus entry was measured in one of two ways: the first was via epi-fluorescence microscopy and the second was by a microplate reader. In the first case, the percentage of cells infected by SARS-CoV-2 pseudovirus was quantified by calculating the ratio of cells expressing GFP to the total number of cells. Cells were imaged using a Nikon Eclipse Ti (Nikon Instruments) inverted microscope equipped with an Andor Technologies iXon em+ EMCCD camera (Andor Technologies). Cells were maintained at 37 °C and 5% CO_2 using a Tokai Hit (Tokai-Hit) stage top incubator and imaged using a 10x objective Pan Fluor NA 0.3 (Nikon Instruments) at 24, 48, and 72 h time points after pseudovirus transductions. In some cases, nuclei were stained using Hoechst prior to imaging to facilitate counting total cell numbers. The total number of cells and the number of cells expressing GFP were manually counted in randomly selected 65 μm by 65 μm imaging windows in ImageJ. The percentage of cells infected was calculated by taking the ratio of the number of cells expressing GFP to the total number of cells. Results were normalized to untreated control samples.

For studies using a microplate reader, HEK293T-hsACE2 cells were seeded in 96-wells optic-bottom black cell culture plates, maintained for 24 h at 37 °C with 5% CO_2 and transduced with pseudoviruses harboring SARS-CoV-2 spike proteins. After 4 h incubation at 37 °C unbound virions were removed by washing thrice with PBS, and cells were further cultured for 72 h at 37 °C with 5% CO_2 . After 72 h supernatant was removed and cells were washed carefully with PBS. 100 μL of PBS was added to each well and fluorescence was measured with Varioskan LuX microplate reader (ex = 480, em = 530). Results were normalized to untreated control samples.

Acquisition of Vimentin Released from Neutrophils: To assess whether vimentin may be acquired from the extracellular environment,

supernatant from PMA stimulated neutrophils was added to the vim-null mEF. To do so, blood was obtained from healthy volunteers (protocol number for human blood draw: R-I-002/231/2019) and neutrophils were isolated by gradient density separation with the use of Polymorphprep. Isolated neutrophils were counted and transferred to Eppendorf tubes containing DMEM at concentration 6×10^5 cells mL^{-1} . 100 nm of PMA was added to neutrophils for 30 min at 37 °C. After incubation, cells were centrifuged and the supernatant was collected. The supernatant was positive for DNA and elastase (data not shown), confirming the neutrophils successfully underwent NETosis. Next, 100 μL of supernatant was added to a prewashed well with 1.5×10^4 vim-null mEFs in a black 96-well glass-bottom plate for 30 min. In the next step, cells were washed three times, fixed, and immunofluorescently stained as described above.

Endocytosis Model: To examine the interaction between extracellular vimentin and the SARS-CoV-2 virus, a coarse-grained molecular dynamics-based 3D model was developed, modeling the role of extracellular vimentin as an attachment factor. The model consisted of the cell membrane, extracellular vimentin, the angiotensin-converting enzyme 2 (ACE2) receptor, the SARS-CoV-2 virus, and the interactions between them. A portion of the cell membrane (approximately 500 nm \times 500 nm in area) was modeled as a tethered membrane with a bending rigidity of 40 $k_B T$. Based on prior experiments,^[47] the extracellular vimentin was considered to be a 40 nm semiflexible filament, bound to the surface of the cell membrane. For simplicity, it was assumed that the SARS2 virus was fully bound to the ACE2 receptor: the spike-ACE2 interaction was given a stiff harmonic spring as ACE2 has a high affinity towards spike protein.^[1] The SARS-CoV-2 virus was designed as a 100 nm diameter elastic viral spherical shell, and the viral shell was decorated with 200 spikes (an upper bound estimate), each containing sticky sites that bind to extracellular vimentin through an attractive Lennard–Jones potential. For excluded volume interactions, soft-core repulsion springs were implemented, should any two particles begin to overlap. Each simulation was run for a total of 10^8 simulation units corresponding to 500 ms. A degree of membrane wrapping metric was defined to reflect membrane curvature as a measure of the depth of the bowl generated by the cell membrane. Specifically, the distance between the height of the cell membrane (far from the bowl) versus the height of the deepest invagination of the membrane bowl was measured: this value was then normalized by the total height of the SARS-CoV-2 virus, 120 nm. (See Experimental Section for full details on the model.)

Statistical Methods: Data are presented as mean values \pm SEM unless otherwise stated. Each experiment was performed a minimum of two times unless otherwise stated. The unpaired, two-tailed Student's t-test at the 95% confidence interval was used to determine statistical significance. Denotations: * $P \leq 0.05$; ** $P < 0.01$; *** $P < 0.001$; NS, $P > 0.05$.

Supporting Information

Supporting Information is available from the Wiley Online Library or from the author.

Acknowledgements

The authors acknowledge Robert Goldman, Karen Ridge, and Nav Singh for insightful discussions. This work was supported by NSF MCB 2032861 award to A.E.P. and J.M.S., NIH R35 GM142963 award to A.E.P., NIH GM136259 award to P.A.J., and the National Science Center of Poland: UMO-2020/01/0/NZ6/00082 awarded to R.B. D.G. acknowledges funding from Syracuse University SOURCE grant. The authors also acknowledge Michael Bates and the Blatt Bioluminescence Center for use of the LSM 980, which was supported by NIH S10 OD026946-01A1.

Conflict of Interest

The authors declare no conflict of interest.

Author Contributions

L.S. and M.S. contributed equally to this work. L.S., M.S., R.B., and A.P. performed and analyzed the SARS-CoV-2 pseudovirus transduction studies. D.G. and D.I. contributed to pseudovirus transduction analysis. L.S. performed the vimentin neutralization assay. L.S., M.S., J.R., N.M., and A.P. performed extracellular vimentin staining. R.B., P.J., and R.C. performed and analyzed dynamic light scattering experiments. F.B. performed and analyzed the atomic force microscopy measurements. S.G. and J.M.S. developed the endocytosis model and analysis. K.P., P.J., J.M.S., J.R., R.B., and A.P. wrote the manuscript. R.B. and A.P. initiated and oversaw the entire project. R.B. and A.P. are co-corresponding authors.

Data Availability Statement

The data that support the findings of this study are available from the corresponding author upon reasonable request.

Keywords

cell membranes, endocytosis, extracellular vimentin, pseudoviruses, SARS-CoV2, spike proteins

Received: September 15, 2021

Revised: October 29, 2021

Published online: December 5, 2021

- [1] D. Wrapp, N. Wang, K. S. Corbett, J. A. Goldsmith, C. L. Hsieh, O. Abiona, B. S. Graham, J. S. McLellan, *Science* **2020**, 367, 1260.
- [2] A. C. Walls, Y.-J. Park, M. A. Tortorici, A. Wall, A. T. McGuire, D. Veelsler, *Cell* **2020**, 183, 1735.
- [3] A. Synowiec, A. Szczepański, E. Barreto-Duran, L. K. Lie, K. Pyrc, *Clin. Microbiol. Rev.* **2021**, 34, e00133.
- [4] F. Hikmet, L. Méar, Å. Edvinsson, P. Micke, M. Uhlén, C. Lindskog, *Mol. Syst. Biol.* **2020**, 16, e9610.
- [5] J. A. Aguiar, B. J.-M. Tremblay, M. J. Mansfield, O. Woody, B. Lobb, A. Banerjee, A. Chandiramohan, N. Tiessen, Q. Cao, A. Dvorkin-Gheva, S. Revill, M. S. Miller, C. Carlsten, L. Organ, C. Joseph, A. John, P. Hanson, R. C. Austin, B. M. McManus, G. Jenkins, K. Mossman, K. Ask, A. C. Doxey, J. A. Hirota, *Eur. Respir. J.* **2020**, 56, 2001123.
- [6] Y. J. Hou, K. Okuda, C. E. Edwards, D. R. Martinez, T. Asakura, K. H. Dinnon 3rd, T. Kato, R. E. Lee, B. L. Yount, T. M. Mascenik, G. Chen, K. N. Olivier, A. Ghio, L. V. Tse, S. R. Leist, L. E. Gralinski, A. Schäfer, H. Dang, R. Gilmore, S. Nakano, L. Sun, M. L. Fulcher, A. Livraghi-Butrico, N. I. Nicely, M. Cameron, C. Cameron, D. J. Kelvin, A. de Silva, D. M. Margolis, A. Markmann, L. Bartelt, R. Zumwalt, F. J. Martinez, S. P. Salvatore, A. Borczuk, P. R. Tata, V. Sontake, A. Kimple, I. Jaspers, W. K. O'Neal, S. H. Randell, R. C. Boucher, R. S. Baric, *Cell* **2020**, 182, 429.
- [7] N. Z. Cuervo, N. Grandvaux, *Elife* **2020**, 9, e61390.
- [8] J. L. Daly, B. Simonetti, K. Klein, K. E. Chen, M. K. Williamson, C. Antón-Plágaro, D. K. Shoemark, L. Simón-Gracia, M. Bauer, R. Hollandi, U. F. Greber, P. Horvath, R. B. Sessions, A. Helenius, J. A. Hiscox, T. Teesalu, D. A. Matthews, A. D. Davidson, B. M. Collins, P. J. Cullen, Y. Yamauchi, *Science* **2020**, 370, 861.
- [9] T. M. Clausen, D. R. Sandoval, C. B. Spliid, J. Pihl, H. R. Perrett, C. D. Painter, A. Narayanan, S. A. Majowicz, E. M. Kwong, R. N. McVicar, *Cell* **2020**, 183, 1043.
- [10] M. A. Tortorici, A. C. Walls, Y. Lang, C. Wang, Z. Li, D. Koerhuis, G. J. Boons, B. J. Bosch, F. A. Rey, R. J. de Groot, D. Veelsler, *Nat. Struct. Mol. Biol.* **2019**, 26, 481.
- [11] C. S. Teo, J. J. Chu, *J. Virol.* **2014**, 88, 1897.
- [12] J. Yang, L. Zou, Y. Yang, J. Yuan, Z. Hu, H. Liu, H. Peng, W. Shang, X. Zhang, J. Zhu, X. Rao, *Sci. Rep.* **2016**, 6, 38372.
- [13] X. B. Chang, Y. Q. Yang, J. C. Gao, K. Zhao, J. C. Guo, C. Ye, C. G. Jiang, Z. J. Tian, X. H. Cai, G. Z. Tong, T. Q. An, *Vet. Res.* **2018**, 49, 75.
- [14] W. W. Wang, L. Zhang, X. C. Ma, J. M. Gao, Y. H. Xiao, E. M. Zhou, *Bingdu Xuebao* **2011**, 27, 456.
- [15] Z. J. Wang, C. M. Xu, Z. B. Song, M. Wang, Q. Y. Liu, P. Jiang, Y. F. Li, J. Bai, X. W. Wang, *Virus Res.* **2018**, 243, 110.
- [16] Q. Zhang, D. Yoo, *Vet. Microbiol.* **2015**, 177, 229.
- [17] P. Turkki, M. Laajala, M. Flodstrom-Tullberg, V. Marjomaki, *J. Virol.* **2020**, 94, e01393.
- [18] K. Kobayashi, S. Koike, *J. Biomed. Sci.* **2020**, 27, 23.
- [19] Y. T. Yu, S. C. Chien, I. Y. Chen, C. T. Lai, Y. G. Tsay, S. C. Chang, M. F. Chang, *J. Biomed. Sci.* **2016**, 23, 14.
- [20] W. Sungnak, N. Huang, C. Bécaivin, M. Berg, R. Queen, M. Litvinukova, C. Talavera-López, H. Maatz, D. Reichart, F. Sampaziotis, *Nat. Med.* **2020**, 26, 681.
- [21] C. G. Ziegler, S. J. Allon, S. K. Nyquist, I. M. Mbanjo, V. N. Miao, C. N. Tzouanas, Y. Cao, A. S. Yousif, J. Bals, B. M. Hauser, *Cell* **2020**, 181, 1016.
- [22] M. Kasper, P. Stosiek, *Eur. Arch. Oto-Rhino-Laryngol.* **1990**, 248, 53.
- [23] H. Herrmann, U. Aebi, *Cold Spring Harbor Perspect. Biol.* **2016**, 8, a018242.
- [24] H. Lodish, A. Berk, S. L. Zipursky, P. Matsudaira, D. Baltimore, J. Darnell, *Molecular Cell Biology*, 4th ed., W.H. Freeman, New York **2000**.
- [25] R. Khandpur, C. Carmona-Rivera, A. Vivekanandan-Giri, A. Gizinski, S. Yalavarthi, J. S. Knight, S. Friday, S. Li, R. M. Patel, V. Subramanian, P. Thompson, P. Chen, D. A. Fox, S. Pennathur, M. J. Kaplan, *Sci. Transl. Med.* **2013**, 5, 178ra40.
- [26] E. Moisan, D. Girard, *J. Leukocyte Biol.* **2006**, 79, 489.
- [27] N. Mor-Vaknin, A. Punturieri, K. Sitwala, D. M. Markovitz, *Nat. Cell Biol.* **2003**, 5, 59.
- [28] T. A. Fasipe, S. H. Hong, Q. Da, C. Valladolid, M. T. Lahey, L. M. Richards, A. K. Dunn, M. A. Cruz, S. P. Marrelli, *Stroke* **2018**, 49, 2536.
- [29] B. Xu, R. M. deWaal, N. Mor-Vaknin, C. Hibbard, D. M. Markovitz, M. L. Kahn, *Mol. Cell. Biol.* **2004**, 24, 9198.
- [30] A. E. Patteson, A. Vahabikashi, R. D. Goldman, P. A. Janmey, *BioEssays* **2020**, 42, 2000078.
- [31] D. S. Fudge, S. Schorno, *Cells* **2016**, 5, 25.
- [32] F. Danielsson, M. K. Peterson, H. Caldeira Araujo, F. Lautenschlager, A. K. B. Gad, *Cells* **2018**, 7, 147.
- [33] Z. Kang, S. Luo, Y. Gui, H. Zhou, Z. Zhang, C. Tian, Q. Zhou, Q. Wang, Y. Hu, H. Fan, D. Hu, *Int. J. Obes.* **2020**, 44, 2479.
- [34] H. R. Thiam, S. L. Wong, R. Qiu, M. Kittisopikul, A. Vahabikashi, A. E. Goldman, R. D. Goldman, D. D. Wagner, C. M. Waterman, *Proc. Natl. Acad. Sci. U. S. A.* **2020**, 117, 7326.
- [35] A. Garg, P. F. Barnes, A. Porgador, S. Roy, S. Wu, J. S. Nanda, D. E. Griffith, W. M. Girard, N. Rawal, S. Shetty, R. Vankayalapati, *J. Immunol.* **2006**, 177, 6192.
- [36] D. Huet, M. Bagot, D. Loyaux, J. Capdevielle, L. Conraux, P. Ferrara, A. Bensusan, A. Marie-Cardine, *J. Immunol.* **2006**, 176, 652.
- [37] Z. Chen, L. Yang, Y. Cui, Y. Zhou, X. Yin, J. Guo, G. Zhang, T. Wang, Q. Y. He, *Oncotarget* **2016**, 7, 67387.
- [38] M. Shigyo, T. Kuboyama, Y. Sawai, M. Tada-Umezaki, C. Tohda, *Sci. Rep.* **2015**, 5, 12055.

- [39] M. Shigyo, C. Tohda, *Sci. Rep.* **2016**, *6*, 28293.
- [40] E. D. Hay, *Dev. Dyn.* **2005**, *233*, 706.
- [41] J. P. Thiery, H. Acloque, R. Y. Huang, M. A. Nieto, *Cell* **2009**, *139*, 871.
- [42] A. Satelli, S. Li, *Cell. Mol. Life Sci.* **2011**, *68*, 3033.
- [43] A. Satelli, I. Batth, Z. Brownlee, A. Mitra, S. Zhou, H. Noh, C. R. Rojas, H. Li, Q. H. Meng, S. Li, *Oncotarget* **2017**, *8*, 49329.
- [44] D. Frescas, C. M. Roux, S. Aygun-Sunar, A. S. Gleiberman, P. Krasnov, O. V. Kurnasov, E. Strom, L. P. Virtuoso, M. Wrobel, A. L. Osterman, M. P. Antoch, V. Mett, O. B. Chernova, A. V. Gudkov, *Proc. Natl. Acad. Sci. U. S. A.* **2017**, *114*, E1668.
- [45] S. W. Li, C. Y. Wang, Y. J. Jou, T. C. Yang, S. H. Huang, L. Wan, Y. J. Lin, C. W. Lin, *Sci. Rep.* **2016**, *6*, 25754.
- [46] N. Zhu, D. Zhang, W. Wang, X. Li, B. Yang, J. Song, X. Zhao, B. Huang, W. Shi, R. Lu, *N. Engl. J. Med.* **2020**, *382*, 727.
- [47] B. Hwang, H. Ise, *Genes Cells* **2020**, *25*, 413.
- [48] P. A. Janmey, D. R. Slochower, Y.-H. Wang, Q. Wen, A. Cēbers, *Soft Matter* **2014**, *10*, 1439.
- [49] G. Schafer, L. M. Graham, D. M. Lang, M. J. Blumenthal, M. Bergant Marusic, A. A. Katz, *J. Virol.* **2017**, *91*, e00307.
- [50] V. Lalioti, S. González-Sanz, I. Lois-Bermejo, P. González-Jiménez, Á. Viedma-Poyatos, A. Merino, M. A. Pajares, D. Pérez-Sala, *bioRxiv* **2021**.
- [51] H. Hagiwara, Y. Aotsuka, Y. Yamamoto, J. Miyahara, Y. Mitoh, *Hum. Antibodies* **2001**, *10*, 77.
- [52] I. Babic, E. Nurmemmedov, V. M. Yenugonda, T. Juarez, N. Nomura, S. C. Pingle, M. C. Glassy, S. Kesari, *Hum. Antibodies* **2018**, *26*, 95.
- [53] D. G. Thalla, P. Jung, M. Bischoff, F. Lautenschläger, *Int. J. Mol. Sci.* **2021**, *22*, 7469.
- [54] D. H. Gong, Y. Dai, S. Chen, X. Q. Wang, X. X. Yan, Y. Shen, J. Liu, Z. K. Yang, J. Hu, L. J. Yu, *Int. J. Cardiol.* **2019**, *283*, 9.
- [55] M. Hoffmann, H. Kleine-Weber, S. Schroeder, N. Krüger, T. Herrler, S. Erichsen, T. S. Schiergens, G. Herrler, N.-H. Wu, A. Nitsche, *Cell* **2020**, *181*, 271.
- [56] A. Bayati, R. Kumar, V. Francis, P. S. McPherson, *J. Biol. Chem.* **2021**, *296*, 100306.
- [57] H. Wang, P. Yang, K. Liu, F. Guo, Y. Zhang, G. Zhang, C. Jiang, *Cell Res.* **2008**, *18*, 290.
- [58] G. Simmons, J. D. Reeves, A. J. Rennekamp, S. M. Amberg, A. J. Piefer, P. Bates, *Proc. Natl. Acad. Sci. U. S. A.* **2004**, *101*, 4240.
- [59] M. Kawase, K. Shirato, L. van der Hoek, F. Taguchi, S. Matsuyama, *J. Virol.* **2012**, *86*, 6537.
- [60] Y.-W. Kam, Y. Okumura, H. Kido, L. F. Ng, R. Bruzzone, R. Altmeyer, *PLoS One* **2009**, *4*, e7870.
- [61] T. Tang, M. Bidon, J. A. Jaimes, G. R. Whittaker, S. Daniel, *Antiviral Res.* **2020**, *178*, 104792.
- [62] Y. Inoue, N. Tanaka, Y. Tanaka, S. Inoue, K. Morita, M. Zhuang, T. Hattori, K. Sugamura, *J. Virol.* **2007**, *81*, 8722.
- [63] N. S. Sharif-Askari, F. S. Sharif-Askari, M. Alabed, M.-H. Temsah, A. S. Heialy, Q. Hamid, R. Halwani, *Mol. Ther.–Methods Clin. Dev.* **2020**, *18*, 1.
- [64] S. Lukassen, R. L. Chua, T. Trefzer, N. C. Kahn, M. A. Schneider, T. Muley, H. Winter, M. Meister, C. Veith, A. W. Boots, B. P. Hennig, M. Kreuter, C. Conrad, R. Eils, *EMBO J.* **2020**, *39*, e105114.
- [65] J. A. Müller, R. Groß, C. Conzelmann, J. Krüger, U. Merle, J. Steinhart, T. Weil, L. Koepke, C. P. Bozzo, C. Read, G. Fois, T. Eiseler, J. Gehrman, J. van Vuuren, I. M. Wessbecher, M. Frick, I. G. Costa, M. Breunig, B. Grüner, L. Peters, M. Schuster, S. Liebau, T. Seufferlein, S. Stenger, A. Stenzinger, P. E. MacDonald, F. Kirchhoff, K. M. J. Sparrer, P. Walther, H. Lickert, T. F. E. Barth, M. Wagner, J. Münch, S. Heller, A. Kleger, *Nat. Metab.* **2021**, *3*, 149.
- [66] W. Trypsteen, J. Van Cleemput, W. V. Snippenberg, S. Gerlo, L. Vandekerckhove, *PLoS Pathog.* **2020**, *16*, e1009037.
- [67] S. Klein, M. Cortese, S. L. Winter, M. Wachsmuth-Melm, C. J. Neufeldt, B. Cerikan, M. L. Stanifer, S. Boulant, R. Bartenschlager, P. Chlanda, *Nat. Commun.* **2020**, *11*, 5885.
- [68] Y. Liu, L.-M. Yan, L. Wan, T.-X. Xiang, A. Le, J.-M. Liu, M. Peiris, L. L. Poon, W. Zhang, *Lancet Infect. Dis.* **2020**, *20*, 656.
- [69] J. L. Walker, B. M. Bleaken, A. R. Romisher, A. A. Alnwibit, A. S. Menko, *Mol. Biol. Cell* **2018**, *29*, 1555.
- [70] F. W. Lam, Q. Da, B. Guillory, M. A. Cruz, *J. Immunol.* **2018**, *200*, 1718.
- [71] I. S. Batth, L. Dao, A. Satelli, A. Mitra, S. Yi, H. Noh, H. Li, Z. Brownlee, S. Zhou, J. Bond, *Int. J. Cancer* **2020**, *147*, 3550.
- [72] H. Noh, Q. Zhao, J. Yan, L. Y. Kong, K. Gabrusiewicz, S. Hong, X. Xia, A. B. Heimberger, S. Li, *Cancer Lett.* **2018**, *433*, 176.
- [73] P. J. Drobinski, A. C. Bay-Jensen, A. S. Siebuhr, M. A. Karsdal, in *Increased Serum Levels of Circulating Vimentin and Citrullinated Vimentin are Differently Regulated by Tocilizumab and Methotrexate Monotherapies in Rheumatoid Arthritis, Arthritis & Rheumatology*, Wiley, Hoboken, NJ USA **2020**.
- [74] S. H. Huang, F. Chi, L. Peng, T. Bo, B. Zhang, L. Q. Liu, X. Wu, N. Mor-Vaknin, D. M. Markovitz, H. Cao, Y. H. Zhou, *PLoS One* **2016**, *11*, e0162641.
- [75] F. Lam, C. Brown, S. Ronca, *FASEB J.* **2021**, *35*.
- [76] J. Yang, S. J. Petitjean, M. Koehler, Q. Zhang, A. C. Dumitru, W. Chen, S. Derclaye, S. P. Vincent, P. Soumillion, D. Alsteens, *Nat. Commun.* **2020**, *11*, 1.
- [77] Z. Li, J. Wu, B. Yuan, K. Dinno, L. Mo, F. Zhou, Y. Dong, K. Gully, R. Baric, R. Graham, Y. Xu, R. Chen, *Clin. Cancer Res.* **2021**, *27*, P35.
- [78] Y. Zheng, J. Zhang, M. Huang, T. Wang, X. Qu, L. Wu, J. Song, W. Wang, Y. Song, C. Yang, *Anal. Chem.* **2020**, *92*, 9895.
- [79] S. Das, V. Ravi, A. Desai, *Virus Res.* **2011**, *160*, 404.
- [80] N. C. Santos, A. C. Silva, M. A. Castanho, J. Martins-Silva, C. Saldanha, *ChemBioChem* **2003**, *4*, 96.